# Dynamic Control of Underactuated Manipulators with Free-Swinging Passive Joints in Cartesian Space

**Jin-Ho Shin* and Ju-Jang Lee**

Department of Electrical Engineering
Korea Advanced Institute of Science and Technology (KAIST)
373-1, Kusong-dong, Yusong-gu, Taejon, 305-701, KOREA
TEL : +82-42-869-3432,5432, FAX : +82-42-869-3410
E-mail : jhshin@odyssey.kaist.ac.kr, jjlee@ee.kaist.ac.kr

## Abstract

*In this paper, a feedback linearizing decoupling dynamic control scheme of nonholonomic underactuated manipulators with free-swinging passive joints is proposed in Cartesian space where the task is planned. The presented control scheme does not require any braking process of passive joints. The presented dynamic control scheme has so-called "dynamic singularities" in the controller. Therefore, the singularities must be avoided in the path-planning so as to guarantee the availability of the control scheme. Singularity-free desired paths in Cartesian space avoiding the dynamic singularities are obtained through a computer simulation. Simulation results for a three-link planar manipulator with one passive joint are presented to show the feasibility of the proposed control scheme with the singularity-free desired trajectory.*

## 1 Introduction

The control of nonholonomic mechanical systems, i.e., systems with non-integrable differential constraints on generalized coordinates, has attracted growing attention in recent years. In fact, many nonholonomic systems naturally fit into the category of *underactuated* mechanisms, defined as systems in which the dimension of the configuration space exceeds that of the control input space. Examples of nonholonomic underactuated systems are acrobots, cart-pole systems, mobile-based robots with no base actuators, a car with $n$-trailers with passive joints, robot manipulators with failed actuators, free-flying space manipulators without jets or momentum wheels where the base can be considered as a virtual passive linkage in inertial space, underactuated spacecrafts, underactuated surface vessels, hyper-redundant (snake-like) robots with passive joints, underwater vehicles with no base actuators, legged robots with passive joints, etc.

In the control of fully-actuated manipulators, desired control forces and/or torques may be applied to each joint by actuators. These are *actuated joints* or *active joints*. There are however manipulators with *unactuated joints* or *passive joints* that may not have actuators at some joints. In usual, a robot manipulator that has fewer number of joint actuators than the number of its total joints is so-called an *underactuated manipulator* [1]-[8]. It is well-known fact that an articulated underactuated manipulator with passive joints satisfies a second-order nonholonimic constraint which is a non-integrable constraint on the acceleration [2][6].

The advantages of using such underactuated systems reside in the fact that they weigh less, and consume less energy than their fully-actuated counterparts, and allow a more compact design and simpler control and communication scheme. The underactuated robot concept is also useful for the reliability or fault-tolerant design of fully-actuated manipulators working with dangerous materials or in remote or hazardous areas such as space, underwater, nuclear power plants, etc. [2][4]-[9].

The term *free-swinging failure* refers to a hardware or software fault in a robotic manipulator that causes the loss of torque (or force) on a joint. After a free-swinging failure, the failed joint moves freely under the influence of external forces and gravity [8].

Several studies on the control of underactuated manipulators have been performed [1]-[8]. The research on the control of underactuated manipulators in Cartesian space without braking the passive joints has not been yet studied actively and so it is currently a fresh problem.

In this paper, a feedback linearizing decoupling dynamic control scheme of underactuated manipulators is proposed in Cartesian space where the task is planned. This control scheme is based on the cancellation of the nonlinear terms in the dynamics by a nonlinear feedback. The considered underactuated manipulator has the active joints equipping the independent actuators and the free-swinging passive joints without both the actuators and the brakes. The presented control scheme does not require any braking process of passive joints. The presented dynamic feedback control scheme has so-called *dynamic singularities* in the controller, which is similar to those of free-flying space manipulators. The dynamic singularities depend on the dynamic parameters as well as the kinematic parameters. Therefore, the singularities must be avoided in the path-planning in order to guarantee the availability of the control scheme. Singularity-free desired paths in Cartesian space avoiding the dynamic singularities are obtained via a computer simulation.

To show the feasibility of the proposed control scheme with the singularity-free desired trajectory, simulation results for a three-link planar manipulator with one passive joint are shown.

## 2 Kinematics and Dynamics of Underactuated Manipulators

The kinematics in position level to map the position in joint space to that in Cartesian space is written as follows: $p_e = f(q) \in \Re^m$ where $p_e \in \Re^m$ is the manipulator's end-effector position and orientation vector with respect to the base frame in Cartesian space, $q \in \Re^n$ is the manipulator's joint position vector in joint space and $f(q) \in \Re^m$ is the nonlinear sinusoidal function of the joint variable vector.

Differentiating the kinematics with respect to time, the Jacobian relationship to map the joint velocity in joint space to the linear and angular velocity of the end-effector with respect to the base frame in Cartesian space is obtained as follows:

$$\dot{p}_e = J(q)\,\dot{q} \quad \in \Re^m \tag{1}$$

where $J(q) \in \Re^{m\times n}$ is the Jacobian matrix of the robot manipulator, which is usually the function of the joint variable vector and the kinematic parameters such as link length, etc.

The Jacobian matrix can be partitioned as follows:

$$J(q) = \begin{pmatrix} J_a(q) & J_p(q) \end{pmatrix} \in \Re^{m\times n} \tag{2}$$

where $J_a(q) \in \Re^{m\times r}$ is the active part of the Jacobian matrix and $J_p(q) \in \Re^{m\times p}$ is the passive part of it. Here, $n(=r+p)$ is the number of the total joints, $r$ is the number of the actuated or active joints and $p$ is the number of the unactuated or passive joints.

Using the Lagrangian formulation, the dynamic equation of a $n$-link rigid open-chain underactuated manipulator with $r$-actuated joints and $p$-unactuated joints can be written in joint space as follows:

$$M(q)\ddot{q} + C(q,\dot{q})\dot{q} + G(q) = \tau = B\tau_a = \begin{pmatrix} \tau_a \\ O_p \end{pmatrix} \tag{3}$$

where $q = (q_a^T\ q_p^T)^T \in \Re^{(n=r+p)}$ is the joint variable, $q_a \in \Re^r$ is the $r$-actuated (active) joints, $q_p \in \Re^p$ is the $p$-unactuated (passive) joints, $M(q) \in \Re^{n\times n}$ is the symmetric, bounded, positive definite inertial matrix, $C(q,\dot{q})\dot{q} \in \Re^{n\times n}$ presents the centrifugal and Coriolis torques, $G(q) \in \Re^n$ is the vector of gravitational torques, $B \in \Re^{n\times r}$ is the input matrix, $\tau = (\tau_a^T\ O_p^T)^T \in \Re^n$ is the control torque input vector, $\tau_a \in \Re^r$ is the actual control input applied to the active joints, and $O_p \in \Re^p$ is the zero input vector applied to the passive joints.

This equation (3) can be partitioned as follows.

$$\begin{pmatrix} M_{aa} & M_{ap} \\ M_{pa} & M_{pp} \end{pmatrix} \begin{pmatrix} \ddot{q}_a \\ \ddot{q}_p \end{pmatrix} + \begin{pmatrix} F_a \\ F_p \end{pmatrix} = B\tau_a = \begin{pmatrix} \tau_a \\ O_p \end{pmatrix} \tag{4}$$

where $F(q,\dot{q}) = (F_a^T\ F_p^T)^T = C(q,\dot{q})\dot{q} + G(q)$.

In equation (4), a second-order nonholonomic constraint [2][6] which is a non-integrable constraint on the acceleration is found as follows.

$$M_{pa}\,\ddot{q}_a + M_{pp}\,\ddot{q}_p + F_p = O_p \quad \in \Re^p. \tag{5}$$

In order to perform control in Cartesian space, it is necessary to obtain a dynamic model relating the Cartesian space variables' accelerations to the torques applied at the active joints.

Differentiating (1) with respect to time, the relationship to map the joint acceleration to the acceleration of the end-effector is obtained as follows.

$$\ddot{p}_e = \dot{J}(q)\,\dot{q} + J(q)\,\ddot{q} \quad \in \Re^m. \tag{6}$$

Multiplying (3) by $JM^{-1}$, we have

$$J\ddot{q} + JM^{-1}F = JM^{-1}\begin{pmatrix} \tau_a \\ O_p \end{pmatrix} = \tilde{J}_a\tilde{M}_{aa}^{-1}\tau_a \tag{7}$$

where $\tilde{M}_{aa}$ and $\tilde{J}_a$ are called the *effective inertial matrix* and *effective Jacobian matrix* of the robot arm, respectively, and defined as follows,

$$\tilde{M}_{aa} = M_{aa} - M_{ap}M_{pp}^{-1}M_{pa} \quad \in \Re^{r\times r}, \tag{8}$$

$$\tilde{J}_a = J_a - J_pM_{pp}^{-1}M_{pa} \quad \in \Re^{m\times r} \tag{9}$$

and $D(q)$ called *decoupling matrix* [5] for the system is defined by

$$D(q) = JM^{-1}B = \tilde{J}_a\tilde{M}_{aa}^{-1} \quad \in \Re^{m\times r}. \tag{10}$$

Substituting (6) into (7), we can obtain the following differential equation,

$$\ddot{p}_e - b(q,\dot{q}) = D(q)\tau_a \quad \in \Re^m \tag{11}$$

where $b(q,\dot{q}) = \dot{J}(q,\dot{q})\dot{q} - J(q)M^{-1}(q)F(q,\dot{q}) \in \Re^m$.

## 3 Dynamic Control of Underactuated Manipulators in Cartesian Space

A feedback linearizing decoupling dynamic controller is made by the following form

$$\tau_a = D^{\#}(q)(v - b(q,\dot{q})) \quad \in \Re^r \tag{12}$$

where $D^{\#}(q) \in \Re^{r\times m}$ is the pseudoinverse matrix of $D(q) \in \Re^{m\times r}$.

The property for the pseudoinverse matrix is shown as follows.

*Property 1:* Let's define a $m$ by $r$ matrix $A$. Then the pseudoinverse matrix of $A$ is $A^{\#} \in \Re^{r\times m}$. The following three cases according to the magnitude relation of $m$ and $r$ are shown.

1. When $m < r$ ; $AA^{\#} = I_m$, $A^{\#}A \neq I_r$, $A^{\#} = A^T(AA^T)^{-1}$, where $I_m \in \Re^{m\times m}$ and $I_r \in \Re^{r\times r}$ is the identity matrices.
2. When $m > r$ ; $A^{\#}A = I_r$, $AA^{\#} \neq I_m$, $A^{\#} = (A^TA)^{-1}A^T$.
3. When $m = r$ ; $A^{\#}A = AA^{\#} = I_r = I_m$, $A^{\#} = A^{-1}$.

The availability of the above controller (12) is guaranteed by the following assumptions.

**Assumption 1:** *It is assumed that $r \geq m$ in the design of a controller.*

*Remark 1:* From Property 1, It is easily found that the number ($r$) of the actuated joints of a manipulator which is greater than or equal to the $m$-dimensional configuration space are needed to control the $m$-dimensional configuration of the end-effector in Cartesian space by driving $r$-actuacted joints. Therefore, the above assumption is necessary to guarantee that $D(q)D^{\#}(q) = I_m$.

**Assumption 2:** *In the controller (12), it is assumed that the pseudo inverse of $D(q)$, $D^{\#}(q)$, exists for all joint configurations of the maipulator during the control process. In other words, it is assumed that $D(q)$ is of full rank or nonsingular for all joint configurations.*

*Remark 2:* Since $r \geq m$ from Assumption 1, the fact that $D^{\#}(q)$ exists is the same that $DD^T \in \Re^{m\times m}$ is invertible or of full rank from case 1 of Property 1.

*Remark 3:* Since the singularities of the decoupling matrix $D(q)(= \tilde{J}_a\tilde{M}_{aa}^{-1})$ depend on both the kinematic

parameters and the dynamic parameters, unlike the singularities for fixed-base manipulators, they are called *dynamic singularities.*

With the control law (12), the differential equation (11) can be rewritten by

$$\begin{aligned} \ddot{p}_e &= b(q,\dot{q}) + D(q)\,\tau_a \\ &= b(q,\dot{q}) + D(q)\,D^{\#}(q)(v - b(q,\dot{q})) = v \end{aligned} \quad (13)$$

The outer loop input $v$ is developed by $v = \ddot{p}_d - K_v\dot{e} - K_p e$ where $K_v \in \Re^{m\times m}$ and $K_p \in \Re^{m\times m}$ are positive definite diagonal constant gain matrices. The Cartesian tracking error $e$ is also denoted as follows, $e = p_e - p_{e_d} \in \Re^{m\times m}$ where $p_{e_d} \in \Re^{m\times m}$ is a desired trajectory of the end-effector specified in Cartesian space.

We now summarize the control system as follows:

$$\ddot{p}_e = b(q,\dot{q}) + D(q)\,\tau_a \quad (14)$$

$$\tau_a = D^{\#}(q)(v - b(q,\dot{q})) \quad (15)$$

$$v = \ddot{p}_d - K_v\dot{e} - K_p e \quad (16)$$

**Theorem 1:** *Under Assumption 1 and 2, if we apply the control law (15) and (16) to the underactuated manipulator system (9), then the tracking errors are globally exponentially stable.*

**Proof :** Substituting (16) into (13), the closed-loop error dynamics is found as follows:

$$\ddot{e} + K_v\dot{e} + K_p e = 0. \quad (17)$$

Therefore, the tracking errors $e$ and $\dot{e}$ are globally exponentially stable.

The proof of Theorem 1 is completed. ■

## 4 Path-Planning Avoiding Dynamic Singularities

As mentioned before, the above assumptions (Assumption $1 \sim 2$) must be satisfied to guarantee the availability of the presented controller. Once the manipulator is within the inside of the singular configurations, Assumption 2 is not guaranteed. Therefore, a path-planning avoiding the dynamic singularities is needed.

In order to control the manipulator in Cartesian space, the desired trajectory $p_{e_d}(t)$ of the manipulator's end-effector should be planned in Cartesian space. The kinematics mapping from joint space to Cartesian space is many-to-one mapping, but the inverse kinematics mapping from Cartesian space to joint space is one-to-many mapping. Thus, one Cartesian point has many joint configurations.

The decoupling matrix $D(q)$ is the nonlinear sinusoidal function of the joint position vector $q$. Therefore, the singularities of $D(q)$ must be shown in joint space. The set of singular points found in joint space can be shown as the regions in Cartesian space via the kinematics. Some regions shown in Cartesian space corresponding to those shown in joint space may be the singular regions or may not be the singular regions as known by the inverse kinematics which is one-to-many mapping. We call these regions "*semi-singular regions*". The terminology "*semi*-singular regions" means that it is doubtful whether those are singular or not. On the other hand, it is guaranteed that the regions which are nonsingular in joint space are always nonsingular regions in Cartesian space. Therefore, the desired path of the end-effector avoiding the dynamic singularities should be constituted within the inside of the regions in Cartesian space that the nonsingular regions in joint space are transformed by the kinematics. Then, the desired path of the end-effector which is made so can guarantee the avoidance of the singularities.

We now presents a path-planning procedure avoiding the singularities as follows.

1. Obtain the dynamic singularity regions such that $|\mathrm{Det}(D(q)\,D^T(q))| \le \epsilon$ for almost all joint configurations in joint space for the given manipulator, where $\mathrm{Det}(D\,D^T)$ represents the determinant of the matrix $D(q)\,D^T(q) \in \Re^{m\times m}$.

   *Remark 4:* Since $r \ge m$ as assumed in Assumption 1, Remark 2 shows that the existence of $D^{\#}(q)$ is the same that $\mathrm{Det}(D(q)\,D^T(q)) \neq 0$. Since the investigation of the singularities is usually performed numerically in digital computers, it is very difficult that $\mathrm{Det}(D\,D^T)$ becomes exactly zero. Therefore, it is necessary that the criterion $\epsilon$ which is a very small positive constant in the neighborhood of zero is specified by designers.

2. Show the semi-singularity regions in Cartesian space corresponding to the singularity regions in joint space by means of the kinematics. Show also the singularity-free regions in Cartesian space corresponding to the nonsingular regions in joint space.

3. Make a desired path or trajectory within the inside of the nonsingular regions in Cartesian space.

## 5 Simulation Study

The underactuated manipulator to be simulated is a three-link planar manipulator with one passive joint: $n = 3$, $r = 2$, $p = 1$, $m = 2$ and so $r = m$. The simulated three-link planar underactuated manipulator is shown in Fig. 1. It is here assumed that this passive joint is freely swinging and does not have both the its own actuator and the brake. It is assumed that there is no frictions in the manipulator's joints in this simulation. It is also assumed that there is no joint limit on each joint, namely, the joint angles can be moved from 0 (rad) to $2\pi$ (rad). The numerical physical parameters of the simulated robot manipulator are shown in Table I. The links are modeled as a uniform thin rod so that the moments of inertia are determined by $I_i = \frac{1}{12}m_i L_i^2$ and the length $L_{ci}$ by $\frac{L_i}{2}(i = 1,2,3)$.

Table I: Parameters of the simulated three-link robot

| $L_1(m)$ | $L_2(m)$ | $L_3(m)$ | $m_1(kg)$ | $m_2(kg)$ | $m_3(kg)$ |
|---|---|---|---|---|---|
| 1 | 1 | 1 | 1 | 1 | 1 |

The simulation includes the singularity-free trajectory planning and the feedback dynamic control tracking the planned trajectory.

### 5.1 Singularity-Free Trajectory Planning

The desired trajectories avoiding the dynamic singularities are planned for three cases of a three-link planar manipulator according to the location of the passive joint in this simulation study. The first case (Case 1) is the case that the third joint is unactuated or passive. The second one (Case 2) is the case that the second joint is

passive. The case that the first joint is passive is the last one (Case 3).

In this simulation, we also use two types of the desired paths of the end-effector in Cartesian space: One is the straight line ($x_d(t) = \alpha\, y_d(t) + \beta$); and the other is the circle ($x_d(t) = R\cos(\theta_d(t)) + x_{dc}$, $y_d(t) = R\sin(\theta_d(t)) + y_{dc}$). The type of the trajectory tracking these paths used in this simulation is a quintic polynomial as follows: For the straight line motion, $y_d(t) = a_0 + a_1 t + a_2 t^2 + a_3 t^3 + a_4 t^4 + a_5 t^5$. For the circular motion, $\theta_d(t) = b_0 + b_1 t + b_2 t^2 + b_3 t^3 + b_4 t^4 + b_5 t^5$. The parameters of the trajectories are obtain by the initial and final conditions.

Now, the singularity-free regions for the above three cases are shown by the simulation. A small positive criterion constant $\epsilon$ shown in Remark 4 in order to determine the singularity numerically is selected as $\epsilon = 10^{-7}$ in the following simulations.

#### 5.1.1 Case 1 : The third joint ($q_3$) is passive

For the manipulator with the robot parameters given in Table I, the singularity-free regions in Cartesian space or task space or operational space are shown in Fig. 2. For the manipulator with the parameters given in the following tables (Table II and Table III), these region are shown in Fig. 3 and Fig. 4, respectively. The moments of inertia $I_i$ and the lengths $L_{ci}$ of the links are modeled by the same method as before as follows: $I_i = \frac{1}{12} m_i L_i^2$, $L_{ci} = \frac{L_i}{2} (i = 1, 2, 3)$.

Table II: Parameters of the simulated three-link robot

| $L_1(m)$ | $L_2(m)$ | $L_3(m)$ | $m_1(kg)$ | $m_2(kg)$ | $m_3(kg)$ |
|---|---|---|---|---|---|
| 1.5 | 1 | 0.5 | 3 | 2 | 1 |

Table III: Parameters of the simulated three-link robot

| $L_1(m)$ | $L_2(m)$ | $L_3(m)$ | $m_1(kg)$ | $m_2(kg)$ | $m_3(kg)$ |
|---|---|---|---|---|---|
| 0.5 | 1.5 | 1 | 1 | 3 | 2 |

As shown before, two types of the desired trajectories are planned to simulate the presented control scheme with application to the manipulator with the link parameter values given in Table I. For the straight line motion, the desired initial and final position in X-Y plane are $(x_{di}, y_{di}) = (0.5, -0.5)$ and $(x_{df}, y_{df}) = (-0.5, 0.5)$, respectively. The desired initial and final velocities and accelerations are $(\dot{x}_{di}, \dot{y}_{di}) = (\ddot{x}_{di}, \ddot{y}_{di}) = (\dot{x}_{df}, \dot{y}_{df}) = (\ddot{x}_{df}, \ddot{y}_{df}) = (0, 0)$. The total execution time ($t_f$) is $t_f = 5(sec)$. In the equation $x_d(t) = \alpha\, y_d(t) + \beta$, $\alpha = 1, \beta = 0$. The parameters of a quintic polynomial for $y_d(t)$ are as follows: $a_0 = -0.5, a_1 = 0, a_2 = 0, a_3 = 0.08, a_4 = -0.024, a_5 = 0.00192$. Therefore, the desired path $x_d(t) = y_d(t)$ is used in the control simulation. For the circular motion, $(x_{di}, y_{di}) = (0.5, 0)$ and $(x_{df}, y_{df}) = (0.5, 0)$. $(\dot{x}_{di}, \dot{y}_{di}) = (\ddot{x}_{di}, \ddot{y}_{di}) = (\dot{x}_{df}, \dot{y}_{df}) = (\ddot{x}_{df}, \ddot{y}_{df}) = (0, 0)$, $t_f = 5(sec)$. In the equation $x_d(t) = R\cos(\theta(t))$, $y_d(t) = R\sin(\theta(t))$, the radius of the circle is $R = 0.5$. The parameters of a quintic polynomial for $\theta(t)$ are as follows: $b_0 = 0, b_1 = 0, b_2 = 0, b_3 = 0.502655, b_4 = -0.150796, b_5 = 0.012064$. Therefore, the desired path $x_d^2(t) + y_d^2(t) = R^2$ is used in the control simulation. The task is that the robot end-effector circulates one time along the specified circle.

#### 5.1.2 Case 2 : The second joint ($q_2$) is passive

For the robot manipulator of Table I, Fig. 5 shows the singularity-free regions when the second joint is passive.

#### 5.1.3 Case 3 : The first joint ($q_1$) is passive

For the robot manipulator of Table I, the singularity-free regions are shown in Fig. 6 when the first joint is passive.

In Fig. 2 ~ Fig. 6, the "*semi*-singular regions" mean that those regions may be singular or may not be singular as mentioned in Section 4. On the other hand, it is guaranteed that the nonsingular regions in these figures are always nonsingular for all joint configurations.

We can find the fact that the singularity-free regions are very various according to the robot parameter values such as link length, link mass, location of center of mass of each link and link inertia. It is also obtained that the singularity regions are much different according to the location of the passive joints. In Fig. 4, all the regions of the total workspace of the given manipulator are the semi-singular regions in Cartesian space, and thus we can say that a Cartesian space control of this manipulator is not always possible.

Now, the dynamic control results tracking the desired trajectories planned in the inside of the singularity-free regions found in the above simulations are shown in the next.

### 5.2 Dynamic Control in Cartesian Space

Simulation results for the controller (15) and (16) are shown in Fig. 7 ~ Fig. 10. We show two cases of the control results according to the direction of the plane which the planar manipulator moves: In other words, the first case is the parallel case to the ground. The perpendicular case to the ground is the second one. In the case that the robot moves in the horizontal plane to the ground, the vector of gravitational torques $G(q)$ in the dynamic equation of the planar manipulator is zero. On the other hand, the vector of gravitational torques $G(q)$ is non-zero in the case that the robot moves in the vertical plane to the ground.

In this simulation, the case that the first and second joints are active and the third joint ($q_3$) is only passive is considered. The numerical parameter values of the simulated manipulator are presented in Table I. The moments of inertia and the lengths of the center of mass of each link are the same as given before.

The actual initial position of the end-effector in X-Y plane is the same as the desired initial position. The used PD gains are $K_p = \mathrm{diag}(1000, 1000), K_v = \mathrm{diag}(2\sqrt{1000}, 2\sqrt{1000})$.

#### 5.2.1 Parallel Plane to Ground : $G(q) = 0$

Fig. 7-(a) ~ Fig. 7-(d) and Fig. 8-(a) ~ Fig. 8-(d) show the control resuts for the straight line motion and the circular motion with a quintic polynomial, respectively.

As shown in Fig. 8-(d), the magnitude of the control torque input is small because $G(q) = 0$ and then the great force to move the passive joint is not necessary.

#### 5.2.2 Perpendicular Plane to Ground : $G(q) \neq 0$

Fig. 9-(a) ~ Fig. 9-(d) and Fig. 10-(a) ~ Fig. 10-(d) show the control resuts for the straight line motion and the circular motion with a quintic polynomial, respectively.

As shown in Fig. 10-(d), the magnitude of the control torque input is large compared to the case of $G(q) = 0$,

because $G(q) \neq 0$ and then the great force to move the passive joint is necessary to overcome the gravitational force. As a result, Fig. 9-(c) and Fig. 10-(c) show that the first joint angle ($q_1$) has very large value, which means that the first link moves the several rounds.

As found in the above simulation results, it has been shown that the presented singularity-free path-planning and dynamic control scheme are feasible and valid.

## 6 Conclusions

The kinematics, dynamics, path-planning and control of underactuated robot manipulators with a second-order nonholonomic constraint have been considered in this paper. A dynamic feedback control scheme of underactuated manipulators has been proposed in Cartesian space. The considered underactuated manipulator has the active joints equipping the independent actuators and the free-swinging passive joints without both the actuators and the brakes. The presented control scheme does not require the braking process of passive joints. For the control in Cartesian space, it can be found that the number of active joints should be greater than or equal to the number of configurational dimension of the robot end-effector in Cartesian space. In order to guarantee the availability of the control law, singularity-free desired paths in Cartesian space avoiding the dynamic singularities have been obtained via the numerical computer simulation.

The feasibility of the proposed control scheme with the singularity-free desired trajectory have been shown through the simulation study for a three-link planar manipulator with one free-swinging passive joint.

The proposed control scheme can be extended for the control of large class of underactuated robot manipulators including spatial redundant manipulators with many passive joints as well as planar underactuated manipulators under the enough dynamic coupling between the active joints and the passive ones.

## References


[1] H. Arai and S. Tachi, "Position Control of a Manipulator with Passive Joints Using Dynamic Coupling," *IEEE Trans. on Robotics and Automation*, Vol. 7, No. 4, pp. 528–534, 1991.

[2] G. Oriolo and Y. Nakamura, "Control of Mechanical Systems with Second-Order Nonholonomic Constraints: Underactuated Manipulators," *Proc. of the 30th Conf. on Decision and Control*, Dec., pp. 2398–2403, 1991.

[3] H. Arai, K. Tanie and S. Tachi, "Dynamic Control of a Manipulator with Passive joints in Operational Space," *IEEE Trans. on Robotics and Automation*, Vol. 9, No. 1, pp. 85–93, 1993.

[4] M. Bergerman, C. Lee and Y. Xu, "A Dynamic Coupling Index for Underactuated Manipulators," *J. of Robotic Systems*, Vol. 12, No. 10, pp.693-707, Oct., 1995.

[5] M. Bergerman, C. Lee and Y. Xu, "Experimental Study of an Underactuated Manipulator," *Proc. of the 1995 IEEE/RSJ Int. Conf. on Intelligent Robots and Systems*, Pittsburgh, PA, USA, Vol. 2, pp. 317–322, 1995.

[6] K. Y. Wichlund, O. J. Sørdalen and O. Egeland, "Control Properties of Underactuated Vehicles," *Proc. of the 1995 IEEE Int. Conf. on Robotics and Automation*, Nagoya, Aichi, Japan, pp. 2009–2014, 1995.

[7] T. Suzuki, M. Koinuma and Y. Nakamura, "Chaos and Nonlinear Control of a Nonholonomic Free-Joint Manipulator," *Proc. of the 1996 IEEE Int. Conf. on Robotics and Automation*, Minneapolis, Minnesota, USA, pp. 2666–2675, 1996.

[8] J. D. English and A. A. Maciejewski, "Fault Tolerance for Kinematically Redundant Manipulators: Anticipating Free-Swinging Joint Failures," *Proc. of the 1996 IEEE Int. Conf. on Robotics and Automation*, Minneapolis, Minnesota, USA, pp. 460–467, 1996.

[9] M. L. Visinsky, J. R. Cavallaro and I. D. Walker, "A Dynamic Fault Tolerance Framework for Remote Robots," *IEEE Trans. on Robotics and Automation*, Vol. 11, No. 4, pp. 477–490, Aug., 1995.


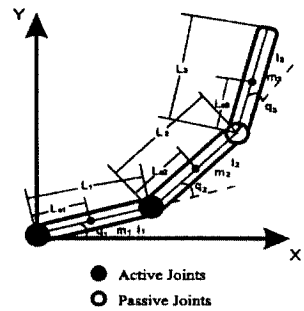


Fig. 1. A three-link planar underactuated manipulator.

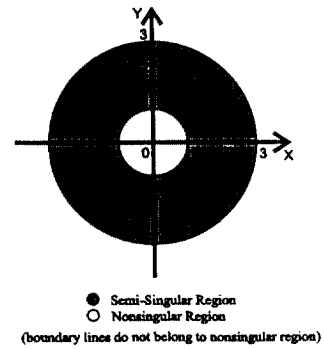


Fig. 2. Semi-singular regions and nonsingular regions (Case 1 and Table I).

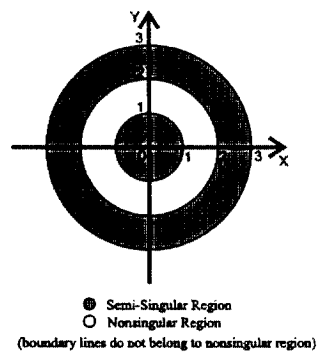


Fig. 3. Semi-singular regions and nonsingular regions (Case 1 and Table II).

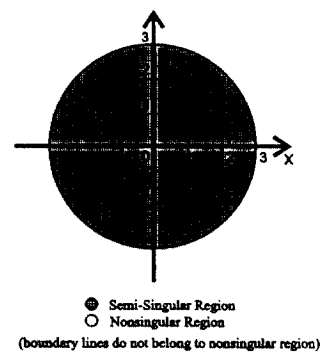


Fig. 4. Semi-singular regions and nonsingular regions (Case 1 and Table III).

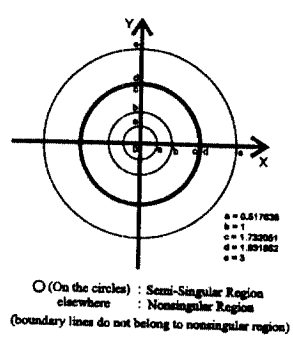


Fig. 5. Semi-singular regions and nonsingular regions (Case 2 and Table I).

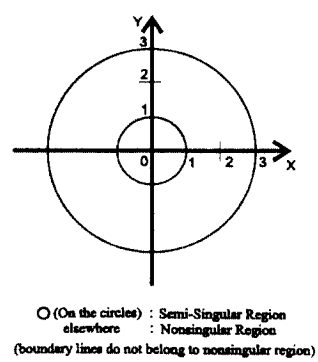


Fig. 6. Semi-singular regions and nonsingular regions (Case 3 and Table I).

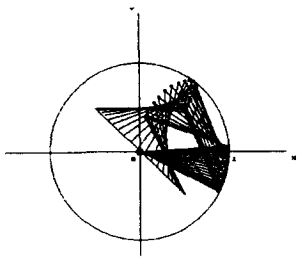

Fig. 7-(a). Snapshot of robot motion.

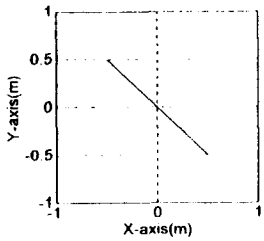


Fig. 7-(b). Actual and desired trajectory of robot end-effector in X-Y plane. (solid line : Actual value; dashed line : desired value)

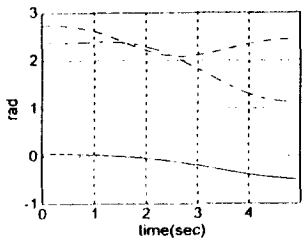


Fig. 7-(c). Each joint angle (rad). (solid line : $q_1$; dashed line : $q_2$; dashdot line : $q_3$)

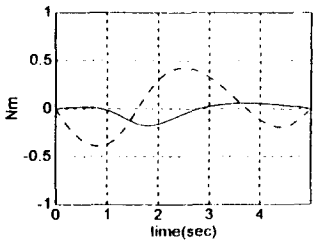


Fig. 7-(d). Control torque input (Nm). (solid line : $\tau_1$; dashed line : $\tau_2$)

Fig. 7. Dynamic control results when $G(q) = 0$ and the desired trajectory is the straight line motion.

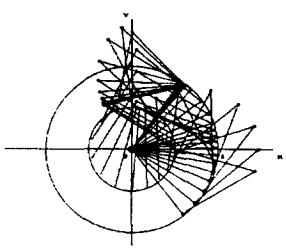

Fig. 8-(a). Snapshot of robot motion.

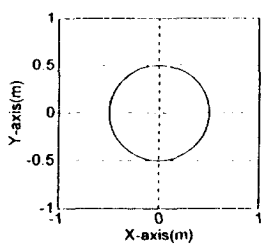


Fig. 8-(b). Actual and desired trajectory of robot end-effector in X-Y plane. (solid line : Actual value; dashed line : desired value)

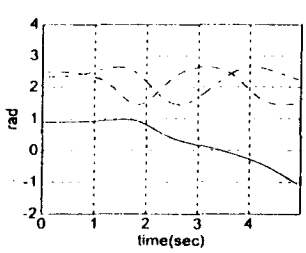


Fig. 8-(c). Each joint angle (rad). (solid line : $q_1$; dashed line : $q_2$; dashdot line : $q_3$)

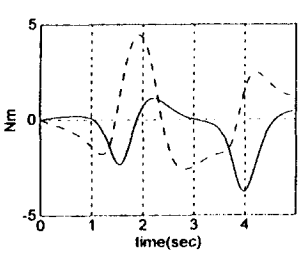


Fig. 8-(d). Control torque input (Nm). (solid line : $\tau_1$; dashed line : $\tau_2$)

Fig. 8. Dynamic control results when $G(q) = 0$ and the desired trajectory is the circular motion.

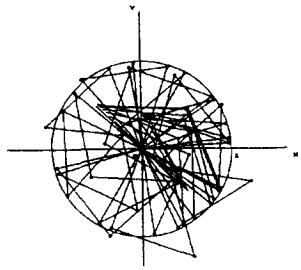

Fig. 9-(a). Snapshot of robot motion.

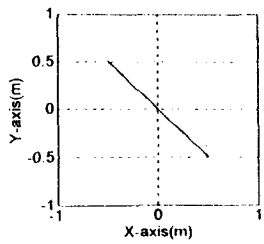


Fig. 9-(b). Actual and desired trajectory of robot end-effector in X-Y plane. (solid line : Actual value; dashed line : desired value)

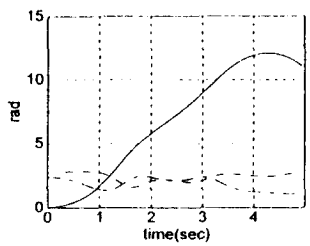


Fig. 9-(c). Each joint angle (rad). (solid line : $q_1$; dashed line : $q_2$; dashdot line : $q_3$)

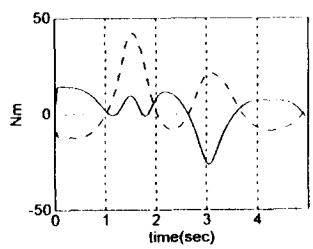


Fig. 9-(d). Control torque input (Nm). (solid line : $\tau_1$; dashed line : $\tau_2$)

Fig. 9. Dynamic control results when $G(q) \neq 0$ and the desired trajectory is the straight line motion.

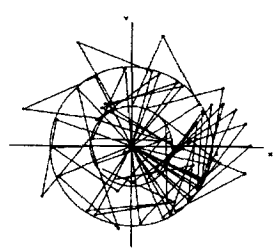

Fig. 10-(a). Snapshot of robot motion.

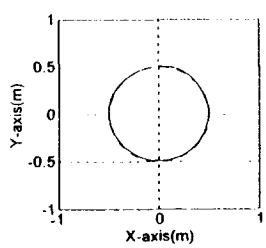


Fig. 10-(b). Actual and desired trajectory of robot end-effector in X-Y plane. (solid line : Actual value; dashed line : desired value)

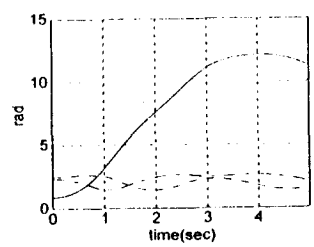


Fig. 10-(c). Each joint angle (rad). (solid line : $q_1$; dashed line : $q_2$; dashdot line : $q_3$)

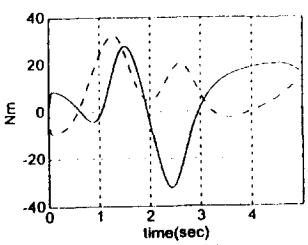


Fig. 10-(d). Control torque input (Nm). (solid line : $\tau_1$; dashed line : $\tau_2$)

Fig. 10. Dynamic control results when $G(q) \neq 0$ and the desired trajectory is the circular motion.